minerals

MDPI

Article

Preliminary Mineralogical Characterization of Branching Selenite Gypsum: New Insights for the Paleoenvironmental Reconstruction and Mechanical Characterization

Chiara Caselle *, Linda Pastero, Simona Cavagna and Sabrina Bonetto

Earth Science Department, Torino University, 10125 Torino, Italy; linda.pastero@unito.it (L.P.); simona.cavagna@unito.it (S.C.); sabrina.bonetto@unito.it (S.B.)
* Correspondence: chiara.caselle@unito.it; Tel.: +39-011-670-5325

Abstract: The present study proposes a characterization of textural and mineralogical features of branching selenite gypsum lithofacies from the Monferrato area (NW Italy). This facies is considered to have appeared during the sequence of the primary lower gypsum of the Messinian Salinity Crisis starting from the sixth stratigraphical cycle, providing a useful tool for stratigraphic correlation throughout the Mediterranean. It is often associated with thick and continuous beds that are exploited by open-pit and underground quarries. We provide the results of a characterization of the non-gypsum minerals that represent approximately 10% in weight of the rock. Mineralogical data were collected with energy-dispersive X-ray spectroscopy (EDS) and X-ray powder diffraction (XRPD) techniques. In addition, a detailed characterization of clay families was performed through dedicated XRPD analyses. Results highlight the presence of detrital minerals (quartz, feldspars and clay minerals), calcite, dolomite and epsomite. Clay analysis registered the existence of five different families (illite, chlorite, smectite and two mixed layers). These mineralogical data suggest that the origin of this lithofacies is connected to both depositional processes and in situ precipitation processes under different conditions of saturation of the brine (respectively undersaturated and supersaturated in sulfates). The mineralogical and textural heterogeneity also represents an important element in controlling the mechanical response of the material and the consequent stability of quarry sites.

Keywords: branching selenite; gypsum; Messinian Salinity Crisis; clay minerals; mechanical characterization; soft rocks

Citation: Caselle, C.; Pastero, L.; Cavagna, S.; Bonetto, S. Preliminary Mineralogical Characterization of Branching Selenite Gypsum: New Insights for the Paleoenvironmental Reconstruction and Mechanical Characterization. *Minerals* **2022**, *12*, 378. https://doi.org/10.3390/min12030378

Academic Editor: Francisco Ruiz

Received: 2 December 2021
Accepted: 15 March 2022
Published: 19 March 2022

1. Introduction

The Earth's geological history records several giant evaporitic events, during which big marine basins were affected by extreme climatic conditions, allowing for the precipitation of enormous masses of salt, gypsum and other evaporitic minerals (e.g., the infra-Cambrian of the Middle East and the Permian of eastern Europe). Among the others, the Messinian Salinity Crisis of the Mediterranean is probably one of the most famous and controversial events due to its recent age and the amount of precipitate rocks despite the very short duration [1]. Several studies have been carried out on Mediterranean Messinian sediment in the last decades, starting from the first discovery of continuous layers of evaporite sediments deep-seated in the Mediterranean basin and the formulation of the model of the desiccated Mediterranean (e.g., [2]). In recent years, studies were mainly addressed to investigate outcropping successions, observed in several onshore locations in Italy, Spain, Greece and Cyprus, and to formulate models to describe this paleo-oceanographic event (e.g., [3–8]).

A largely accepted stratigraphic model was proposed by CIESM (Commission Internationale pour l'Exploration Scientifique de la mer Méditerranée) in 2008 [9]. This model divides the crisis into three stages: during the first stage (5.97–5.60 Ma), we observe the

precipitation of the first gypsum sediments in the most marginal and shallow basins (Primary Lower Gypsum unit, organized in cyclical deposition of marl–gypsum pairs that are considered to be deposited under precessional control). The adjacent deeper parts of the basin experience the deposition of organic-rich shale and dolostone, which has been proven to be coeval with the Primary Lower Gypsum [10]. Both these deposits are then interrupted by an important erosional surface defined as the MES (Messinian erosional surface), which marks the transition from the first to the second stage. The second stage (5.60–5.55 Ma) corresponds to the resedimentation of the Primary Lower Gypsum unit as a chaotic body (Resedimented Lower Gypsum) in the deeper basins. Eventually, the third phase (5.55–5.33 Ma) includes the deposition of hypo-haline lagoon sediments.

The interference between these sedimentary conditions and the dynamic tectonic framework that dominated the European geological scene during Mesozoic and Cenozoic (e.g., Alpine orogenesis and rotation of the Corso–Sardinian block) led to the deposition of a strongly heterogeneous evaporite record, making it difficult to find correlation between different localities. Focusing on the Primary Lower Gypsum unit, Lugli et al., 2010 [11], attempted a large facies correlation throughout the Mediterranean, providing a comprehensive facies description. They proposed the definition of a new facies named "branching selenite", consisting of bottom-grown, small-sized, selenite crystals grouped in branches projecting outward from a common nucleation point and developed under the control of a current-dominated brine flow. Following Lugli et al.'s interpretation, this gypsum facies may be recognized, with little difference, in the sedimentary record of the entire Mediterranean area, with a synchronous comparison in the sixth cycle from the onset of the Crisis.

The same sediments were previously described by Vai and Ricci Lucchi, 1977 [12], in central Italy, as a "nodular and lenticular gypsum" due to the re-elaboration of an initial clastic deposit that was subaerially exposed, developing sabkha features.

In the same years, Sturani (1973) [13] described, in Piedmont, a thick layer of laminated microcrystalline gypsum encasing meter-sized masses of selenite, interpreted as diagenetic. This rock facies was then re-interpreted as the newly described branching selenite facies in association with laminated gypsum (i.e., thin alternance of cumulate gypsum and shales) [11,14].

Following Lugli et al., the "supercone structures" described by Dronkert (1985) [15] in the Sorbas Basin (in Spain) may be considered as a different expression of the same branching selenite facies, with only the branch terminations visible against the host matrix.

The Messinian sediments, providing the availability of large volumes of evaporite minerals, represent an important natural resource for mining exploitation. In particular, gypsum is required as a raw material in a wide range of industrial fields (e.g., building engineering, clinical applications, agriculture and production of paints) and for this reason is exploited by both open-pit and underground quarries all over the world. In underground excavations, mining tunnels can reach lengths of tens of kilometers and both underground and surface stability have to be assured. Due to the large variability of existing gypsum facies and the influence of textural and compositional features on the mechanical response, the assessment of the stability of the quarry environments needs to be carried out on the basis of a facies-specific mechanical characterization [16–18].

As well as other gypsum facies, branching selenite is commonly exploited either in open-pit or underground quarries, since, especially in the sixth cycle, it has good lateral continuity, considerable thicknesses and high gypsum purity. In addition, the synchronous comparison of branching selenite facies in the sixth stratigraphic cycle from the onset of the Crisis has, for mining industries, a specific relevance in orebody reconstruction.

Despite the importance of this rock facies for practical and research purposes, a complete mineralogical description, including clay characterization, has not been accomplished. For this reason, this study proposes a textural and mineralogical description of the features of branching selenite facies of the sixth cycle in the Monferrato domain of the Tertiary

Piedmont Basin, aiming at providing useful information for geological interpretations and geotechnical applications.

2. Geological Framework

The Tertiary Piedmont Basin (TPB), located on the inner side of SW Alps arc, is filled with Upper Eocene to Messinian sediments that stratigraphically overlies a complex tectonic wedge of Alpine, Ligurian and Adria basement units juxtaposed in response to the collision between the Europe and Adria plates (e.g., [19]). The Cenozoic sediments are presently exposed in the southern (Langhe, Alto Monferrato and Borbera Grue domains) and the northern (Torino Hill–Monferrato arc) sectors of the TPB. The relationships between the two outcropping belts are masked by Pliocene-to-Holocene deposits of the Savigliano and Alessandria basins but are well-imaged by seismic profiles [20]. In this framework, thick gypsum bodies from the Messinian Salinity Crisis were observed and described in Monferrato and Langhe domains (Figure 1).

Figure 1. Areal distribution of Messinian gypsum deposits in Piedmont and geographical location of the test sites.

In particular, the stratigraphic succession that includes the primary evaporitic rocks in the Monferrato geological domain was well-described in the correspondence of two quarry sites (Moncalvo and Calliano), where the execution of vertical boreholes allowed for a complete description of the sequence [21].

The sequence starts with a deep-sea marl unit named "S.Agata Fossili Marls". Based on bio-stratigraphic and cycle-stratigraphic data, the onset of the Salinity Crisis was identified within this unit, with the two first stratigraphical cycles of the Crisis under the base of gypsum sediments.

The following geological unit consists of a thick evaporitic succession that counts 13 gypsum/marl pairs, interpreted as cycles controlled by orbital parameters. This unit may be considered as the Primary Lower Gypsum unit of the CIESM model [14]. The first three gypsum cycles consist of thick beds of massive selenite, with average thickness of 10 m. In these layers, selenite gypsum is vertically oriented, twinned crystals with sizes between 3 and 10 cm. The interlayer marl levels have a mean thickness of 2–3 m. The gypsum layer of the fourth cycle (the sixth from the onset of the Crisis) corresponds to the appearance of branching selenite facies and consists of a thick layer of about 10 m. The authors of [14] suggested considering this bed as a key layer (labelled "Sturani Key Bed" (SKB)) since it has particular and well-recognizable features that allow it to be distinguished, physically correlated and mapped throughout the Tertiary Piedmont Basin. Over the SKB, the sequence consists of finer interbedded layers of gypsum and marl, with higher clayey terrigenous input, referred to as "higher evaporitic cycles". The succession is sealed by lagoon sediment (i.e., the third phase in the CIESM model) and more-recent clay sediment [21].

3. Methodologies

The textural and microstructural features of SKB branching selenite in the Monferrato domain were described at different scales. The presence of the underground quarry sites of Moncalvo and Calliano offers an interesting macro-scale observatory, thanks to the exposure of large excavation faces (about 6 m × 6 m at Calliano and 10 m × 10 m at Mocalvo).

Observations performed at this scale were integrated and completed with more-detailed descriptions of hand samples (thanks to the availability of a series of drilling cores) and thin sections. Standard petrographic images were acquired with an Olympus BX4 reflected- and transmitted-polarized-light optical microscope with JENOPTIK ProgResC5 digital color camera. Thin sections were also investigated after carbon-coating with a Cambridge S-360 scanning electron microscope (SEM). Backscattered electron images (BSE) were obtained at an accelerating voltage of 15 kV. The textural and microstructural description was completed with compositional analyses performed with EDS (energy dispersive X-ray spectroscopy) and with the measure of the percentage content of gypsum (in weight) with the thermogravimetry method (details on this procedure can be found in [22]).

In parallel, a detailed characterization of non-gypsum mineralogical content was performed with XRPD (X-ray powder diffraction). A total of 0.5 g of material was reduced in size with a mortar and dissolved in water, modifying the solid/solvent ratio to reach a calcium–sulfate concentration lower than the gypsum solubility (2 g/L at 20 °C). After 24 h, the solution was filtered and the solid residual portion was deposited on glass slices ready for the XRPD analysis, in order to study the insoluble minerals without the interference of the gypsum diffraction pattern.

These powder samples were also analyzed following the standard analysis methods for the characterization of clay minerals. XRPD analyses were repeated before and after the application of treatments with organic molecules (i.e., glycol ethylene) and heating (350 °C and 500 °C). The behavior of different clay minerals in response to these treatments is unique, allowing for the determination of the clay mineralogy. In addition to the "classical" families of clays (i.e., illite, smectite and kaolinite) the presence of interstratified clays (e.g., illite–smectite and kaolinite–smectite) was investigated.

The mixed-layer clay analysis was accomplished with the Python open-source code PYXRD [23], implementing a matrix algorithm specifically developed for the analysis of X-ray diffraction of disordered lamellar structures. The software performs a probability analysis on the XRPD data, returning modelled curves to compare with the measured data and the corresponding percentages of each clay family.

4. Results

4.1. Textural Features

Figure 2 reports three examples of excavation faces where the macroscale features of branching selenite texture are clearly visible. The relative position of the faces in the scheme of the underground quarry are reported in Figure 2a. All the considered faces (Figure 2b–d) show the presence of white lenticular bodies ('branches') surrounded by layers of darker material. The size of the branches is variable, with thicker ones of about 1 m (in this case, mainly in the higher part of the layer) and smaller ones with a thickness of a few decimeters. As illustrated by the schematic representation of the faces in Figure 2e–g, at a more detailed analysis, it appears that the branches are not homogeneous but consist of the juxtaposition of several smaller lenses separated by dark material.

Figure 2. (**a**) Localization of the faces reported in this Figure in the schematized map of the underground tunnels of Calliano quarry. (**b**–**d**) Excavation faces in the Sturani Key Bed that expose the features of branching selenite gypsum. (**e**–**g**) Schematic representation of the main "branches" of gypsum identified in the excavation faces.

An interesting element may be noticed, moreover, by comparing the features of the branches with the spatial orientation in the quarry. Gypsum branches in Figure 2c are, indeed, generally longer and with a higher lateral continuity, while in Figure 2b,d they tend to close laterally. From Figure 2a, we can see that faces in Figure 2b,d are oriented in an E–W direction, while faces in Figure 2c have a N–S direction. The different lateral continuity of the gypsum branches in the different faces can therefore be considered as the consequence of the three-dimensional interference of quarry faces with N–S directed gypsum branches. Figure 2c, being oriented parallel to the branches' elongation, shows their longer axes, while Figure 2b,g cut the branches along their shorter axes, showing their lateral terminations.

At the sample scale, the rock appears to be organized in nodular aggregates composed of mm- to cm-sized gypsum crystals (Figure 3a–c). In the aggregates, the gypsum crystals are closely interlocked, creating a dense structure. Their habit is usually prismatic and several of the crystals present twinning (Figure 3d). Most of the crystals show the presence of inclusions, both fluid and solid inclusions (e.g., terrigenous grains and little gypsum crystals, as shown in Figure 3e).

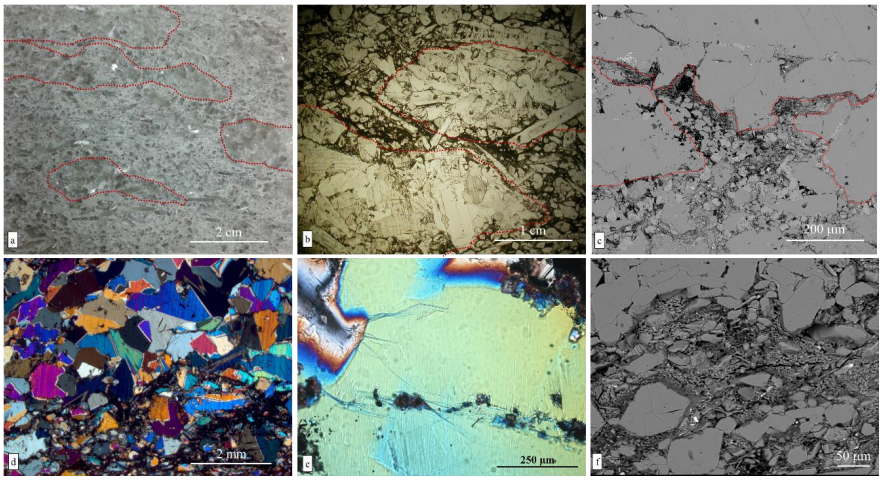

Figure 3. (**a**) Hand sample of branching selenite gypsum, with the presence of lenses of gypsum crystal (the most-evident are identified by red dashed lines) surrounded by finer material that includes gypsum and other components. (**b**) Optical microscope microimage of the gypsum aggregates, compactly interlocked, immersed in a finer material that includes both gypsum and other (darker and finer) minerals. (**c**) SEM-BSE microimage showing the organization of the texture with lenses of gypsum crystals (identified by the red dashed line) surrounded by finer material. (**d**) Optical microscope microimage at crossed nicols showing that gypsum crystals are often twinned and often present inclusions of other minerals. (**e**) Detail of a gypsum crystal in the aggregates, showing inclusions of turbid minerals and little gypsum crystals. (**f**) Detail on the fine-grained material in SEM-BSE.

The nodules are immersed in a finer matrix that consists of two main size classes: the former has an average size of a few tens of microns and is mainly represented by gypsum; the latter is finer and includes a carbonatic cement and terrigenous minerals, mainly with a lamellar habit (Figure 3f).

At this scale, the rock also shows a well-evident iso-orientation of the elongated gypsum crystal in the nodules.

4.2. Compositional Analyses

The thermogravimetric measures of gypsum content returned a percentage of gypsum ranging between 80% and 94% (by weight). As shown in Figure 4, the vertical distribution of these measures shows a certain degree of data dispersion (Figure 4 refers to two reference boreholes denominated S58 and S61). The dispersion of data, however, is consistent with the alternance in the layer of portions with prevalence of "branches" (i.e., with prevalence of gypsum) and portions with prevalence of darker material, in accordance with Figure 2.

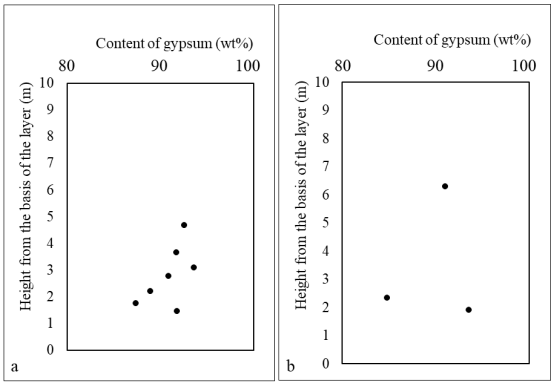

Figure 4. Distribution of percentage of gypsum content (by weight) along the vertical direction of the layer in the two boreholes, denominated S58 (**a**) and S61 (**b**), at Calliano quarry. The y-axis is oriented as the stratigraphic layer, with the top of the layer in the higher part of the Figure.

Along the vertical direction of borehole S61, three samples were taken for compositional analyses with XRPD and EDS. Results are shown in Figure 5, with the additional indication of sample positions in the SKB layer (Figure 5g). XRPD analyses, performed on the non-gypsum portions of the material, revealed the presence of calcite as a common feature in all the samples. In the upper part of the layer (Figure 5a), no other minerals were detected besides gypsum. Consistently, Figure 5b, showing the EDS map performed in the same stratigraphical position, highlights the main rock organization with large crystals of gypsum (in blue in the image) and smaller calcite grains in the pores (in green).

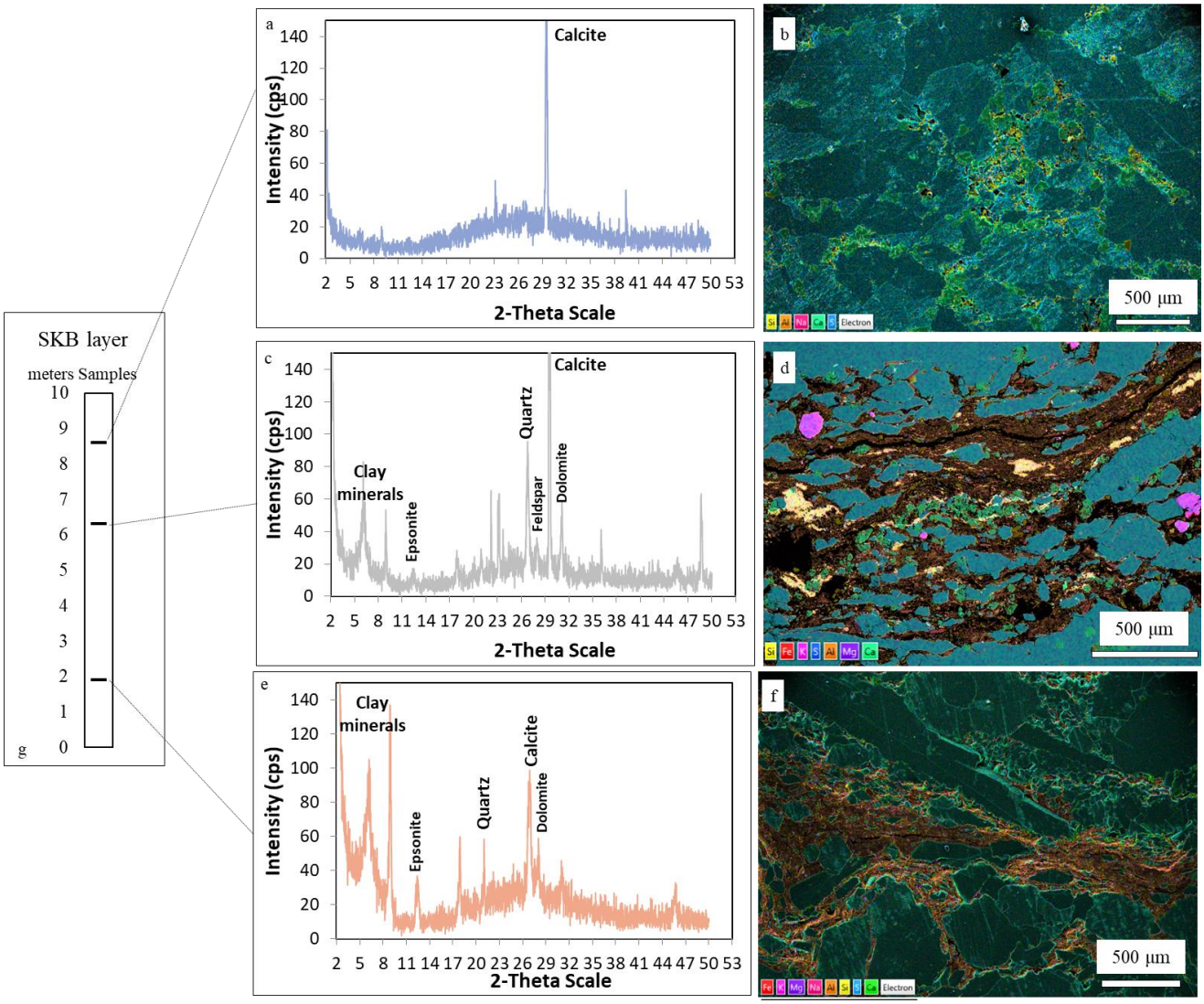

Figure 5. XRPD analyses on the non-gypsum fraction and EDS maps on thin sections of samples from borehole S61. Depth of the samples are: (**a**,**b**): 78 to 79 m; (**c**,**d**): 80.6 to 81 m; (**e**,**f**): 85 to 85.4 m. The SKB layer in this point extends from 77.2 to 87.1 m of depth from the surface. In (**b**,**f**) the EDS maps are superimposed to SEM micrographs acquired in secondary electron mode. The position of the samples in the SKB layer is reported in (**g**).

In the central portion of the layer (Figure 5c,d), aside from calcite, the analyzed powder samples contain quartz, feldspar and clay minerals. Similar to the higher parts of the layer, calcite (in green) mainly consists of grains of a few tens of microns that, in Figure 5d, are organized in layers that locally border the gypsum nodules. On the other hand, clays, feldspars and quartz appear to be fine-grained and represent the main part of the material in the thin layers of the branching structure. As shown in Figure 5d, indeed, these layers

mainly consist of Si (yellow), K (fuchsia), Al (orange), Mg (violet) and Fe (red). The violet mineral in the Figure, consisting of the sum of Fe (red) and S (blue), is pyrite.

This mineralogical composition and organization of the rock (with nodules of gypsum, layers of fine-grained terrigenous minerals and, sometimes, equigranular calcite) is the most common in the rock. It is, indeed, still present in the lower part of the borehole (Figure 5e,f). In these portions of the layer, however, a lower content of calcite is registered by the XRPD patterns. Consistently, the calcite crystals observed in the sample in Figure 5d are not ubiquitous in this rock portion, as confirmed by the absence of calcite in the EDS map in Figure 5f.

The XRPD outputs also showed the presence of dolomite and epsomite (Figure 5c,e).

In order to understand the meaning of these minerals in the depositional context of branching selenite gypsum, we should have a clearer view of their position in the structure of the rock. For this purpose, Figure 6 shows an additional SEM-EDS compositional map of the rock. In the image, the fine-grained material between the gypsum crystals (in orange) consists of two main colors: light blue (i.e., mainly consisting of Si, Al and K) and purple (i.e., mainly consisting of Ca and Mg), suggesting that the dolomite is present in the rock as cement interdigitated to the terrigenous fine-grained material.

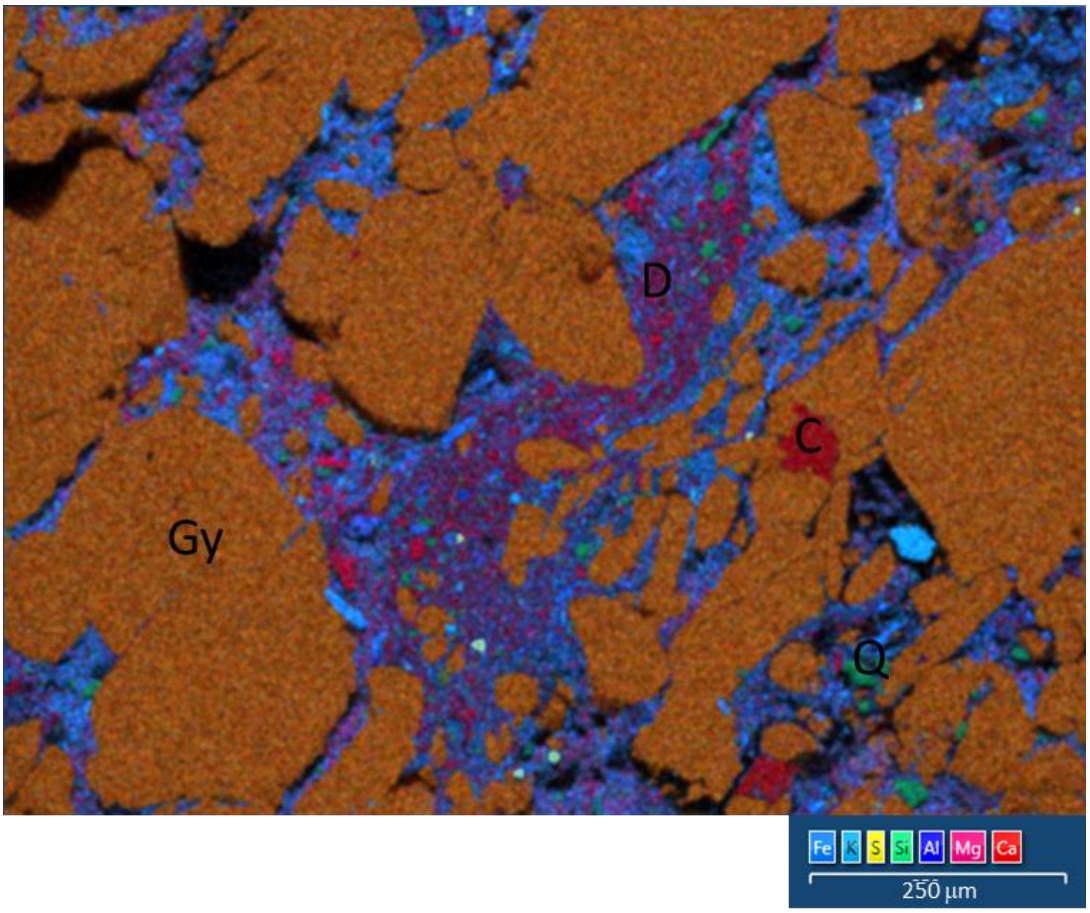

Figure 6. SEM-EDS map of a portion of the rock, showing the presence of a dolomite cement (purple) interdigitated to the fine-grained terrigenous material (light blue).

4.3. Clay Characterization

The classification of clay minerals was performed on the samplesµm seen in Figure 5c–f. Results are reported in Figure 7 and the complete analyses are shown in the supplementary materials (Figure S1).

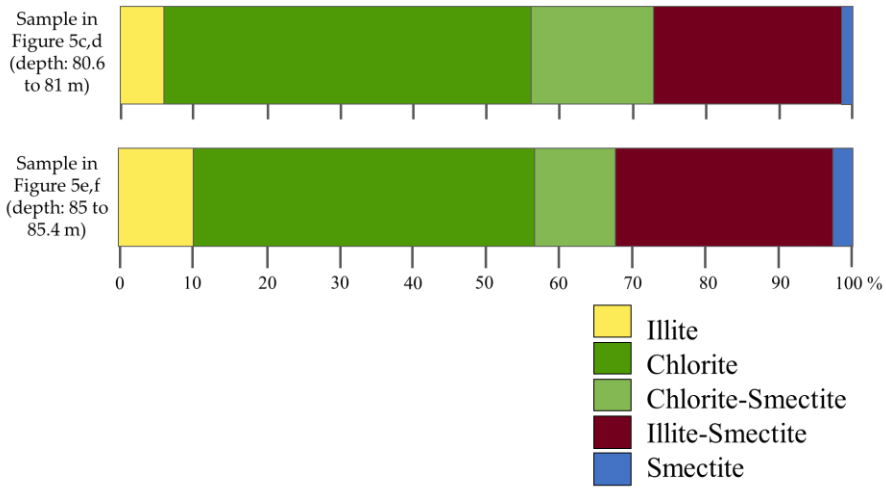

Figure 7. Results of mixed-layer clay classification for samples in Figure 5c,d (depth: 80.6 to 81 m) and in Figure 5e,f (depth: 85 to 85.4 m).

The analysis revealed the presence of five families of clay minerals, that are, in detail:

- illite
- chlorite
- smectite
- a mixed-layer family consisting of three layers of smectite and one of chlorite
- a mixed-layer family consisting of three layers of smectite and one of illite

All these families are consistent with the mean composition identified with EDS analyses: Si, Al, Mg, Fe, Ca and K (Figure 5d–f). Despite some variability, in both samples the higher percentage of phyllosilicates consists of chlorite, followed by the mixed-layer illite–smectite family, that is the main cause of the swelling registered after glycolation. Minor percentages of illite and a mixed-layer smectite–chlorite are observed. Even if present, pure smectite only represents a minor proportion of the samples.

5. Discussion

5.1. Depositional Context of the Branching Selenite Facies

All the most recent studies on branching selenite facies [11,14,24–26] concur in suggesting the existence of a basin-wide hydrologic change driving the synchronous comparison of the branching selenite from the sixth cycle in all the Mediterranean basin. This change in marine conditions is suggested to be a reduction of interchanges with the Atlantic Ocean and an increase in the detrital input and continental runoff and riverine water.

The non-gypsum minerals identified by our new mineralogical data include several phases that are consistent with an abundant detrital apport from the neighboring emerged Alpine chain (i.e., quartz, feldspars, chlorite and calcite). As shown in Figure 5, these minerals are indeed present in the rock as fine detrital material.

However, the XRPD output also showed the presence of other mineral phases (dolomite, pyrite, epsomite, smectite, illite and mixed-layer clays) that suggest the additional existence of in situ processes. The precipitation conditions of these minerals (and of gypsum) are very different, and the coexistence of these phases in the same rock requires discussion. The precipitation of dolomite in marine environment is usually related to anoxic conditions, where the action of sulfate-reducing bacteria reduces the free sulfate ions, inhibiting the precipitation of gypsum. The Ca^{2+} (and Mg^{2+}) ions not involved in the gypsum precipitation may therefore combinate with CO_3^{2-} ions to form dolomite [27]. Under these anoxic and reducing conditions, the availability of reduced sulfide ions allows for precipitation of pyrite.

On the other hand, the precipitation of epsomite (Mg–sulfate bitter salt) requires a marine brine with high sulfate concentration (82,200 mg/l, about 8 times the concentration

required for gypsum precipitation and 30 times the normal seawater concentration). However, in this context, the absence of halite, which in a normal marine evaporation pattern would form before epsomite, suggests that this mineral may also be secondary, possibly due to efflorescence forming on the tunnels' surfaces.

Hence, we have, in the same rock:

- dolomite and pyrite, testifying of unsaturation in sulfates and an anoxic and reducing environment;
- gypsum (and epsomite), testifying of the supersaturation in sulfates.

This suggests that the rock formed during different steps under different brine concentrations.

The most-recently proposed genetical model for branching selenite [26] suggests that this lithofacies formed in a reducing and anoxic seafloor through the syngenetic reprecipitation of pelagic gypsum that nucleated in the water column and deposited at the seafloor. Following the model, the nucleation of gypsum in the water column is cyclically overcome by the apport of detrital material from rivers and other continental sources in response to short-term climate fluctuations, resulting in the deposition of laminated gypsum. However, in the periods of abundance of sulfate nucleation in the water column, the sulfate concentration at the seafloor may become high, resulting in the precipitation of new gypsum crystals in the form of gypsum aggregates.

In this context, the dolomite that cements the detrital fine materials of the rock and the pyrite grains recorded by our XRPD data are consistent with the reducing conditions of the water at the seafloor during the absence of sulfate pelagic rain.

5.2. Clay Minerals

Due to their high reactivity to environmental conditions, clay minerals are often considered to be good indicators of the physical and chemical features of sedimentary environments. In evaporite basins, the elevated ion concentration accelerates the processes of ordering of clay mineral structures since the swelling layers tend to disappear due to the capture of free cations from the highly mineralized brines in the interlayer spaces. As a result, clay minerals such as smectite, mixed-layer minerals and kaolinite are transformed into stable ones (illite, chlorite). With progressive increase of brine concentration, the transformation processes become more intense, causing a decrease in the number of clay mineral species [28,29].

The clay mineral association identified by our XRPD analyses registered the presence of five clay mineral species (illite, chlorite, smectite and two mixed-layers). A similar association confirms an ongoing process of ordering of the clay structures, with the mixed-layer minerals that testify of a process of partial smectitization of a detrital chlorite and a neogenic illite. This is consistent with a depositional environment characterized by the presence of a highly mineralized brine. The revealed clay association is indeed consistent with literature records for evaporitic environments in the calcite–gypsum precipitation stage [28].

5.3. Implications for Quarry Exploitation

As a consequence of the textural organization (i.e., lenses of gypsum—"branches"—with different sizes and orientations), branching selenite is highly heterogeneous in terms of textural, microstructural and compositional features both in the lateral and vertical direction, with an increased abundance of lenses of gypsum aggregates in the higher part of the layer (see Figure 2).

The material heterogeneity may imply significant variability of its physical and mechanical properties. The new mineralogical data reported in this paper offer new insights on this.

In Figure 8, the compositional data presented in this study are compared with the results of mechanical characterizations already published in [16,17,30].

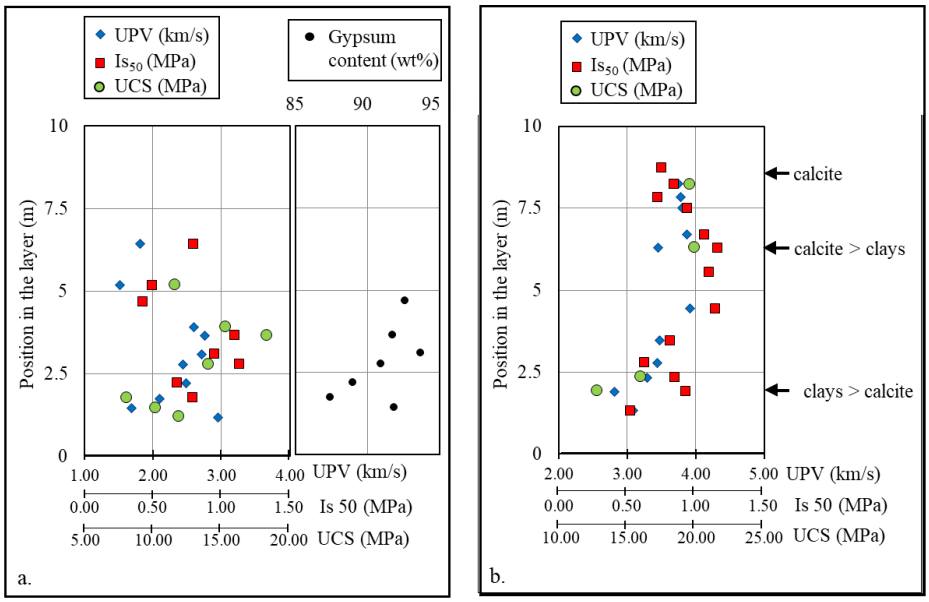

Figure 8. (**a**) Distribution of mechanical and physical parameters (left panel; from [16]) and gypsum content (right panel; from this study) in the S58 borehole. (**b**) Distribution of mechanical and physical parameters in the S61 borehole (from [16]) and position of chemical–mineralogical analyses reported in Figure 5. In the Figure, blue diamonds are the UPV, red squares are the strength index from PLT and green circles are the UCS.

In detail, the mechanical data refer to the measure of three parameters:

- uniaxial compression strength (UCS), i.e., the value of strength of the material under mechanical compression on cylindrical samples;
- strength index (Is_{50}), i.e., the parameter obtained with the point load test (PLT), an expeditive test that measures the failure load of samples between two punctual conical points of contact. This parameter is directly related to the UCS through empirical relationships;
- ultrasonic pulse velocity (UPV), i.e., the velocity of a seismic wave (produced as an ultrasonic pulse) through the material. This value depends on the physical properties of the material (e.g., solid density, porosity, mineralogical composition and presence of cracks) and gives an indirect measure of its mechanical strength.

The totality of these mechanical data homogeneously covers the vertical section of the layer in correspondence of the two boreholes. As can be seen, the data from the different methodologies show similar trends for each borehole.

Figure 8a, showing the results of mechanical tests on borehole S58, reports a quite homogeneous increase of strength and wave velocity from the base of the layer to 4 m. The comparison of these data with the gypsum content (reported in the right panel of Figure 8a) highlights a similarity of trend, suggesting a direct correlation between gypsum percentage and mechanical strength.

Mechanical data in Figure 8b (borehole S61) show, again, an increase of strength and pulse velocity between 0 and 5 m from the basis of the layer. The physical and mechanical values then remain quite stable up to the higher part of the layer (with the exception of Is_{50} from PLT that shows a slight decrease). As suggested by the mineralogical data, synthetically reported on the right of Figure 8b, the lower strength in the lower part of the layer corresponds to a higher concentration of clays and the consequent higher presence of layers or lamellar minerals (i.e., layers of lower strength in the rock structure).

Another element that may affect the mechanical response of branching selenite gypsum is the material anisotropy and the iso-orientation of the crystals. As illustrated in [31], the iso-orientation of crystals in branching selenite gypsum influences the orientation of the failure propagation under stress: the material will show, indeed, a higher propensity

to develop cracks parallel to the preferential orientation of the crystals rather than perpendicular to them. The material description proposed in this paper highlighted how this iso-orientation is identified not only at the sample scale but also at the scale of the quarry site (see Figure 2). As reported by several authors [11,26], this iso-orientation of the branches is organized in a radial pattern, defining asymmetrical conical structures (Figure 9). Hence, a reconstruction of the size and geometrical organization of these conical structures at the local scale may be used to predict the potential orientation of failure propagation, representing an element to consider in the planification of frontal quarry cuts (in open pit configurations) and tunnels (in underground configurations).

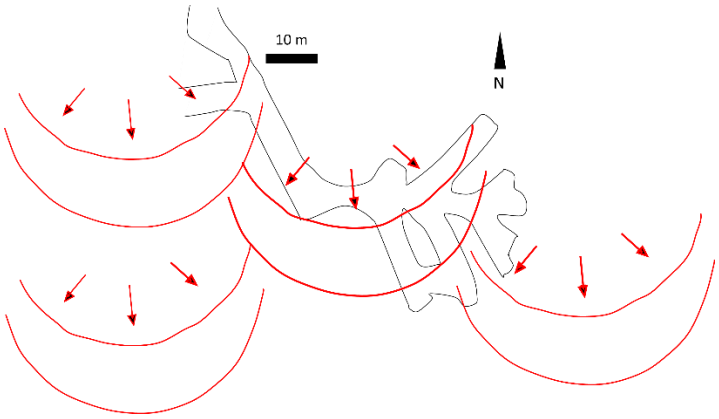

Figure 9. Schematic representation of typical conical orientation of gypsum branches in branching selenite lithofacies following [11,26] (in red) overlaid on the planimetry of the tunnels discussed in Figure 2 (in black).

The absence of good knowledge of the mechanical heterogeneity and anisotropy in rock orebody may result in inaccurate choices of mechanical parameters in the planning, excavation and reclamation phases of quarry exploitation. A geological-based evaluation of the rock orebody is, indeed, important in order to guide the choice of representative values of mechanical strength and able to describe the existence of sub-areas with different mechanical properties in order to avoid strength overestimations that could create severe risk scenarios, or underestimation that would imply the unnecessary large size of underground pillars in cases of good-quality material.

6. Conclusions

The main mineralogical features of branching selenite lithofacies from the SKB layer in the Monferrato domain (Piedmont) were described in this study. The results concur in suggesting that this lithofacies was deposited in the presence of an abundant detrital apport from rivers and other continental sources. Further, the presence of dolomite and epsomite in addition to gypsum suggests that in situ precipitation processes took place during different moments and under different conditions of saturation of the brine (unsaturated and supersaturated, respectively, in sulfates). The revealed clay association, consisting of five different clay families, is consistent with literature records for evaporitic environments. The mineralogical and textural heterogeneity of the rock affects the mechanical response of the material, resulting in strength variability along the vertical and lateral directions.

Supplementary Materials: The following are available online at https://www.mdpi.com/article/10.3390/min12030378/s1, Figure S1: Mixed-layer clays classification. Natural state (a), glycolated (b) and heated (c) XRPD data of sample in Figure 5c-d of the main paper (depth: 80.6 to 81 m) and natural state (d), glycolated (e) and heated (f) XRPD data of sample in Figure 5e-f of the main paper (depth: 85 to 85.4 m). The black curve represents the measured data. Yellow, green, pale-green, brown and blue curves refer to the trends of illite, chlorite, chlorite-smectite mixed-layer, illite-smectite mixed-layer and smectite respectively. The calculated percentages of each mineralogical phase are

reported next to the name of the phase for each sample. The resulting curves (deriving from the convolution of the 5 clay families in the reported percentages) are reported in red. Rp and Rwp values for each sample are reported.

Author Contributions: Conceptualization, S.B.; formal analysis, C.C., L.P. and S.C.; investigation, C.C., L.P. and S.C.; resources, S.B.; data curation, C.C. and L.P.; writing—original draft preparation, C.C.; writing—review and editing, L.P., S.C. and S.B.; visualization, C.C.; supervision, S.B. All authors have read and agreed to the published version of the manuscript.

Funding: This research received no external funding.

Data Availability Statement: Not applicable.

Acknowledgments: The authors desire to thank the private company that made the rock samples used in the presented research available. The authors are also sincerely thankful to the anonymous reviewers that helped to improve the quality of the paper.

Conflicts of Interest: The authors declare no conflict of interest.

References

1. Rouchy, J.M.; Caruso, A. The Messinian Salinity Crisis in the Mediterranean Basin: A Reassessment of the Data and an Integrated Scenario. *Sediment. Geol.* **2006**, *188*, 35–67. [CrossRef]
2. Hsu, K.J.; Cita, M. The origin of the Mediterranean evaporites. *Initial. Rep. Deep. Sea Drill. Proj.* **1973**, *13*, 1203–1231.
3. Butler, R.W.H.; Lickorish, W.H.; Grasso, M.; Pedley, H.M.; Ramberti, L. Tectonics and Sequence Stratigraphy in Messinian Basins, Sicily: Constraints on the Initiation and Termination of the Mediterranean Salinity Crisis. *GSA Bull.* **1995**, *107*, 425–439. [CrossRef]
4. Hilgen, F.; Krijgsman, W. Cyclostratigraphy and Astrochronology of the Tripoli Diatomite Formation (Pre-Evaporite Messinian, Sicily, Italy). *Terra Nova* **1999**, *11*, 16–22. [CrossRef]
5. Krijgsman, W.; Meijer, P.T. Depositional Environments of the Mediterranean "Lower Evaporites" of the Messinian Salinity Crisis: Constraints from Quantitative Analyses. *Mar. Geol.* **2008**, *253*, 73–81. [CrossRef]
6. Dela Pierre, F.; Clari, P.; Bernardi, E.; Natalicchio, M.; Costa, E.; Cavagna, S.; Lozar, F.; Lugli, S.; Manzi, V.; Roveri, M.; et al. Messinian Carbonate-Rich Beds of the Tertiary Piedmont Basin (NW Italy): Microbially-Mediated Products Straddling the Onset of the Salinity Crisis. *Palaeogeogr. Palaeoclimatol. Palaeoecol.* **2012**, *344–345*, 78–93. [CrossRef]
7. Manzi, V.; Lugli, S.; Roveri, M.; Dela Pierre, F.; Gennari, R.; Lozar, F.; Natalicchio, M.; Schreiber, B.C.; Taviani, M.; Turco, E. The Messinian Salinity Crisis in Cyprus: A Further Step Towards a New Stratigraphic Framework for Eastern Mediterranean. *Basin Res.* **2016**, *28*, 207–236. [CrossRef]
8. Sabino, M.; Dela Pierre, F.; Natalicchio, M.; Birgel, D.; Gier, S.; Peckmann, J. The Response of Water Column and Sedimentary Environments to the Advent of the Messinian Salinity Crisis: Insights from an Onshore Deep-Water Section (Govone, NW Italy). *Geol. Mag.* **2021**, *158*, 825–841. [CrossRef]
9. Briand, F. (Ed.) CIESM The Messinian Salinity Crisis from Mega-Deposits to Microbiology—A Consensus Report. In Proceedings of the N° 33 in CIESM Workshop Monographs, Almeira, Spain, 7–10 November 2007; CIESM Publisher: Paris, Monaco, 2008; p. 168.
10. Manzi, V.; Roveri, M.; Gennari, R.; Bertini, A.; Biffi, U.; Giunta, S.; Iaccarino, S.M.; Lanci, L.; Lugli, S.; Negri, A.; et al. The Deep-Water Counterpart of the Messinian Lower Evaporites in the Apennine Foredeep: The Fanantello Section (Northern Apennines, Italy). *Palaeogeogr. Palaeoclimatol. Palaeoecol.* **2007**, *251*, 470–499. [CrossRef]
11. Lugli, S.; Manzi, V.; Roveri, M.; Schreiber, C.B. The Primary Lower Gypsum in the Mediterranean: A New Facies Interpretation for the First Stage of the Messinian Salinity Crisis. *Palaeogeogr. Palaeoclimatol. Palaeoecol.* **2010**, *297*, 83–99. [CrossRef]
12. Vai, G.B.; Ricci Lucchi, F. Algal crusts, autochthonous and clastic gypsum in a cannibalistic evaporite basin: A Case History from the Messinian of Northern Apennines. *Sedimentology* **1977**, *24*, 211–244. [CrossRef]
13. Sturani, C. Messinian Facies in the Piedmont Basin. *Mem. Della Soc. Geol. Ital.* **1976**, *16*, 11–25.
14. Dela Pierre, F.; Bernardi, E.; Cavagna, S.; Clari, P.; Gennari, R.; Irace, A.; Lozar, F.; Lugli, S.; Manzi, V.; Natalicchio, M.; et al. The Record of the Messinian Salinity Crisis in the Tertiary Piedmont Basin (NW Italy): The Alba Section Revisited. *Palaeogeogr. Palaeoclimatol. Palaeoecol.* **2011**, *310*, 238–255. [CrossRef]
15. Dronkert, H. *The Evaporites of the Sorbas Basin*; Instituto de Investigaciones Geológicas Diputación Provincial Universidad de Barcelona: Barcelona, Spain, 1977; Volume 32, pp. 55–76.
16. Caselle, C.; Bonetto, S.; Colombero, C.; Comina, C. Mechanical Properties of Microcrystalline Branching Selenite Gypsum Samples and Influence of Constituting Factors. *J. Rock Mech. Geotech. Eng.* **2019**, *11*, 228–241. [CrossRef]
17. Caselle, C.; Bonetto, S.; Vagnon, F.; Costanzo, D. Dependence of Macro Mechanical Behaviour of Gypsum on Micro-Scale Grain-Size Distribution. *Géotechnique Lett.* **2019**, *9*, 1–9. [CrossRef]
18. Ramon, A.; Caselle, C.; Bonetto, S.M.R.; Costanzo, D.; Alonso, E.E. Effect of Microstructure and Relative Humidity on Strength and Creep of Gypsum. *Rock Mech. Rock Eng.* **2021**, *54*, 4121–4145. [CrossRef]

19. Rossi, M.; Mosca, P.; Polino, R.; Rogledi, S.; Biffi, U. New outcrop and subsurface data in the Tertiary Piedmont Basin (NW-Italy): Unconformity-Bounded Stratigraphic Units and their Relationships with Basin-Modification Phases. *Riv. Ital. Paleontol. Stratigr.* **2009**, *115*, 305–355. [CrossRef]
20. Bertotti, G.; Mosca, P. Late Orogenic Vertical Movements within the Arc of the SW Alps and Ligurian Alps. *Tectonophysics* **2009**, *475*, 117–127. [CrossRef]
21. Dela Pierre, F.; Natalicchio, M.; Lozar, F.; Bonetto, S.; Carnevale, G.; Cavagna, S.; Colombero, S.; Sabino, M.; Violanti, D. The Northernmost Record of the Messinian Salinity Crisis (Piedmont Basin, Italy) Regional Commitee on Mediterranean Neogeone Stratigraphy Interim Colloquium—Torino, 25–28 September 2014. *Geol. Field Trips* **2016**, *8*, 2–58. [CrossRef]
22. Caselle, C.; Bonetto, S.; Comina, C. Comparison of Laboratory and Field Electrical Resistivity Measurements of a Gypsum Rock for Mining Prospection Applications. *Int. J. Min. Sci. Technol.* **2019**, *29*, 603–604. [CrossRef]
23. Dumon, M.; Van Ranst, E. PyXRD v0.6.7: A Free and Open-Source Program to Quantify Disordered Phyllosilicates Using Multi-Specimen X-Ray Diffraction Profile Fitting. *Geosci. Model Dev.* **2016**, *9*, 41–57. [CrossRef]
24. Evans, N.P.; Turchyn, A.V.; Gázquez, F.; Bontognali, T.R.R.; Chapman, H.J.; Hodell, D.A. Coupled Measurements of Δ18O and ΔD of Hydration Water and Salinity of Fluid Inclusions in Gypsum from the Messinian Yesares Member, Sorbas Basin (SE Spain). *Earth Planet. Sci. Lett.* **2015**, *430*, 499–510. [CrossRef]
25. Cipriani, M.; Dominici, R.; Costanzo, A.; D'Antonio, M.; Guido, A. A Messinian Gypsum Deposit in the Ionian Forearc Basin (Benestare, Calabria, Southern Italy): Origin and Paleoenvironmental Indications. *Minerals* **2021**, *11*, 1305. [CrossRef]
26. Natalicchio, M.; Pellegrino, L.; Clari, P.; Pastero, L.; Dela Pierre, F. Gypsum Lithofacies and Stratigraphic Architecture of a Messinian Marginal Basin (Piedmont Basin, NW Italy). *Sediment. Geol.* **2021**, *425*, 106009. [CrossRef]
27. de Lange, G.J.; Krijgsman, W. Messinian Salinity Crisis: A Novel Unifying Shallow Gypsum/Deep Dolomite Formation Mechanism. *Mar. Geol.* **2010**, *275*, 273–277. [CrossRef]
28. Yaremchuk, Y.; Hryniv, S.; Peryt, T.; Vovnyuk, S.; Meng, F. Controls on Associations of Clay Minerals in Phanerozoic Evaporite Formations: An Overview. *Minerals* **2020**, *10*, 974. [CrossRef]
29. Iaremchuk, I.; Tariq, M.; Hryniv, S.; Vovnyuk, S.; Meng, F. Clay Minerals from Rock Salt of Salt Range Formation (Late Neoproterozoic–Early Cambrian, Pakistan). *Carbonates Evaporites* **2017**, *32*, 63–74. [CrossRef]
30. Caselle, C.; Penone, A.; Bonetto, S. Preliminary Mechanical Characterization of Gypsum Rock Using UCS and Point Load Test Correlation. *Geoing. Ambient. E Min.* **2018**, *153*, 60–67.
31. Caselle, C.; Umili, G.; Bonetto, S.; Costanzo, D.; Ferrero, A.M. Evolution of Local Strains Under Uniaxial Compression in an Anisotropic Gypsum Sample. In Proceedings of the Geotechnical Research for Land Protection and Development, Lecco, Italy, 3–5 July 2019; Calvetti, F., Cotecchia, F., Galli, A., Jommi, C., Eds.; Springer International Publishing: Cham, Switzerland, 2020; pp. 454–461.